processes

MDPI

Article

Analysis of the Time Step Influence in the Yearly Simulation of Integrated Seawater Multi-Effect Distillation and Parabolic trough Concentrating Solar Thermal Power Plants

Bartolomé Ortega-Delgado *, Patricia Palenzuela and Diego-César Alarcón-Padilla

CIEMAT-Plataforma Solar de Almería, Ctra. de Senés s/n, 04200 Almería, Spain; patricia.palenzuela@psa.es (P.P.); diego.alarcon@psa.es (D.-C.A.-P.)

* Correspondence: bartolome.ortega@psa.es; Tel.: +34-950-387800; Fax: +34-950-365015

Abstract: The joint demand for power and freshwater is continuously increasing due to population growth, the rise of economic activity, and climate change. Integrated concentrating solar thermal power and desalination (CSP+D) plants may provide a key solution for the pressing freshwater deficit and energy problems in many regions of the world. Simulation tools with an accurate prediction of the yearly electric energy and freshwater production are needed. This paper analyzed the influence of the time step in the annual simulation of a CSP+D plant composed of a seawater multi-effect distillation unit and a parabolic trough concentrating solar thermal power plant, considering the location of Tabernas (Spain). A dynamic simulation tool of this system was developed, implementing the models in Engineering Equation Solver. The annual electricity and water productions obtained for the study case considered were 154 GWh and 3.45 hm^3, respectively, using 5 min time steps, and 94 GWh and 2.1 hm^3, respectively, with 1 h time steps. The results obtained show that a short time step interval (5 min) is recommended when using the detailed CSP model considered, which is prepared for simulation with short time steps. Step times of 1 h lead to excessive errors (about 30% in summer and 100% in winter), which underestimate the actual production.

Keywords: CSP+D; yearly simulation; modeling; simulation tool; multi-effect distillation; parabolic trough; time step influence

Citation: Ortega-Delgado, B.; Palenzuela, P.; Alarcón-Padilla, D.-C. Analysis of the Time Step Influence in the Yearly Simulation of Integrated Seawater Multi-Effect Distillation and Parabolic trough Concentrating Solar Thermal Power Plants. *Processes* **2022**, *10*, 573. https://doi.org/10.3390/pr10030573

Academic Editors: Agustin M. Delgado-Torres and Lourdes García-Rodríguez

Received: 31 January 2022
Accepted: 11 March 2022
Published: 15 March 2022

1. Introduction

Electricity consumption worldwide increased more than threefold in the period from 1980 to 2019, reaching about 22.6 TWh [1]. It is expected a big increase of the demand in developing countries of Asia, Central and South America, and the Middle East for the next decades, particularly in China and India because of their fast-growing economies. These emerging countries will need new structures and systems to acquire both power and freshwater. Classic power production technologies based on fossil fuels such as oil or coal are known to cause environmental problems such as the greenhouse effect and atmospheric pollution. Besides this, population growth is continuously increasing and therefore the global electricity and water demand. This scenario implies the need of using other sources of clean energy such as renewable energy to meet the demand for both water and electricity. The coupling of a concentrating solar power (CSP) plant based on parabolic trough solar collectors with a multi-effect distillation (MED) unit is one of the possible approaches to fulfill these needs and has been analyzed in the scientific literature [2–10].

One distinctive feature of solar power plants is the daily and seasonal variability of solar irradiance and its influence on energy production. Walkenhorst et al. [11] investigated the influence of the minimum period used in the input data of solar irradiance in a specific application. They found underestimations by 27% in the results obtained when using 1 h irradiance data against 1 min data. The influence of solar irradiance variability is especially important in the case of solar thermal concentrating technologies because they only take

advantage of the direct normal component of solar radiation, which in turn is strongly affected by the solar geometry—i.e., the position of the Sun in the sky—and the existing atmospheric conditions. An example of the actual behavior of operational parameters of a parabolic trough solar field is reported by Bonilla et al. [12] concerning a test facility of the Plataforma Solar de Almería (CIEMAT, Spain). The use of automatic control strategies and an appropriate thermal storage system can help to keep constant the main parameters of the power block despite the variability of the solar resource. Nevertheless, when the available thermal energy is not enough to meet the nominal operation of the power block, the turbine works out of the nominal conditions (off-design) with the corresponding efficiency drop.

Other models for PT-CSP plants show the performance of the plant with time variation, i.e., analyze the dynamic response of the system. Lippke [13] studied the part-load behavior of a typical 30 MW_e solar energy-generating system (SEGS) plant without thermal storage. A comparison with actual data from a plant was made for a winter and summer day together with an analysis of the variation of the operating for a day in different seasons. Wagner et al. [14] developed a generic CSP modeling tool, Solar Advisor Model (SAM, NREL), which includes performance models for parabolic troughs, power towers, and dish-Stirling systems. A similar study of the time step influence over the simulation results in PT-CSP plants was performed by Wagner [15], where the Gemasolar concept of using molten salts as heat transfer fluid in solar power tower plants is transferred to parabolic trough plants. Casimiro et al. [16] presented a model for simulating a MED in stationary conditions integrated into a CSP using SAM software environment and 1 h time step for the yearly production calculation. Moser et al. [17] compared the performance of MED and reverse osmosis desalination technologies driven by a CSP plant using the software package INSEL. The annual yield calculation was performed on an hourly basis. Alikulov et al. [18] modeled a hybrid solar-assisted desalination cycle consisting of a parabolic trough solar field and a MED unit. They presented time-series calculations of the optical and field efficiencies together with the generated solar heat using hourly data. Mata-Torres et al. [19] analyzed the transient response of a polygeneration system including a combined parabolic trough solar field and a MED desalination unit. Yearly simulations for the water and power production were performed with hourly meteorological data in the TRNSYS environment. Hoffmann and Dall [20] presented a model for simulating the power and water production of an integrated central receiver plant and multi-effect distillation unit located in Namibia (Africa). They assumed hourly solar input values for the simulations. Results showed that this system was economically viable given the existing water tariffs. Ortega-Delgado et al. [21] developed a simulation tool able to perform detailed yearly simulations of power and water production. A study case was analyzed in Almería (Spain) with different coupling arrangements between the MED unit and the power cycle. The 10 min time steps were used in the simulations to determine the annual yield. Calise et al. [10] compared two CSP+MED plants based on Fresnel and evacuated tube collectors. Simulations were performed in the TRNSYS environment and with time steps of 0.02 h. Askari and Ameri [22] assessed a CSP+D system formed by a Linear Fresnel solar field, Rankine cycle, and a MED desalination unit. They performed a techno-economic analysis using hourly meteorological data. Palenzuela et al. [23] performed a comparative evaluation of the water and power production of a CSP+D plant using MED and RO desalination technologies and considering two different locations: Almería (Spain) and Abu Dhabi (UAE). The yearly simulations were carried out using Matlab and EES software environments with 10 min time steps. Al-Addous et al. [24] analyzed the combined power and water production with a CSP+D plant in the Middle East and North Africa (MENA) region. MED and parabolic trough technologies were considered for the desalination and solar field technologies, respectively. The model was implemented in Ebsilon Professional, and hourly weather data were used for the DNI. Desai et al. [25] presented a techno-economic analysis of a cost-effective concentrating solar collector suitable for applications below 350 °C. This solar field was used to drive an ORC and a MED unit for the joint production of power and water. Simulations using EES were

made for a typical year with 5 min time steps. Other systems powered by solar energy to produce water at a small scale, such as solar still systems, take data every 30 min [26,27].

Despite the great interest in this topic, the analysis of the time step influence on the dynamic response of a dual-purpose power and desalination plant has not been yet investigated to the best of the authors' knowledge. The objective of this work was to study and analyze the dependence on time step in a particular dynamic simulation model for a CSP+D plant to assess its influence on the accuracy of the total electricity and water produced during a full year of operation of the plant. The aim was to help to find a compromise between the computational time required and the accuracy of the simulation results.

2. Methods

The techno-economic assessment of the power and water produced by a CSP+D plant requires a yearly simulation. One of the main input parameters is the typical meteorological year (TMY) that is used to feed the solar thermal plant model to determine the thermal energy delivered to the power block. The TMY is a set of meteorological data in a particular location for one representative year obtained from a minimum period of 10 years. This TMY can be usually obtained from free or commercially available databases that can provide the data with different time steps (time increment between consecutive data). Obviously, the shorter the time steps, the higher the accuracy of the results, but it will also increase the computational time required to perform the simulation task. In this case, the TMY was obtained with Meteonorm software with 10 min data at Plataforma Solar de Almería (2.215 E; 37.06 N) in Tabernas (Spain).

The concentrating solar power plant considered is based on parabolic trough collector technology with thermal storage (two tanks of molten salts) and is based on a typical PT-CSP configuration [28,29], which has been adapted to include the seawater multi-effect distillation plant. These technologies have been selected because they are commercial technologies to produce electricity and water that have been proved as mature and reliable [30,31]. The power cycle consists of a regenerative Rankine cycle with reheat. The total electric power delivered by the power block is 50 MW_e, and the plant is assumed to be located at Plataforma Solar de Almería (2.215 E; 37.06 N) in Tabernas (Spain).

Three subsystems were considered to analyze the influence of the time step in the yearly simulation of the CSP+D system:

The solar thermal subsystem. The solar field consists of 156 loops of parabolic troughs (Eurotrough with SOLEL absorber), each one formed by four solar collector assemblies (SCA) in series, arranged on a North–South axis. Every SCA has 12 solar collector elements (SCE) compound of 36 basic heat collector elements (HCE). A thermal energy storage system consisting of two molten salts tanks is included, which helps to meet the power production to the demand in hours with no insolation available. The thermal energy storage (TES) can provide up to 7.5 h of power block operation at the design conditions. When the heat transfer fluid (HTF) reaches a certain temperature in the solar field, electric energy begins to be generated in the PB thanks to the thermal energy transferred from the HTF to the water through a train of heat exchangers (preheater, steam generator, superheater, and reheater) (Figure 1). The model reported by Llorente et al. [32] was implemented. This model has a high level of detail and is the first model published with thermal storage validated with actual data from an existing plant, showing a good agreement between the results. In addition, this model was benchmarked within the guiSmo project [33], an international group of the SolarPACES Task I dedicated to providing guidelines for the electricity yield analysis of CSP plants.

The model determines the solar time and incidence angle of the solar radiation of the collector, taking as input data the site location (longitude and latitude), meteorological data (local time, DNI, etc.), solar field (collector data), and power block characteristics (turbine efficiency, pump efficiency, etc.). Then, the useful thermal power obtained by the solar field is determined taking into account the DNI, thermal losses in the pipes, and the solar field efficiency. The HTF temperature in each collector (T_1, T_2, T_3, T_4) is then

calculated, and depending on the temperature level and TES state, different operation strategies are followed.

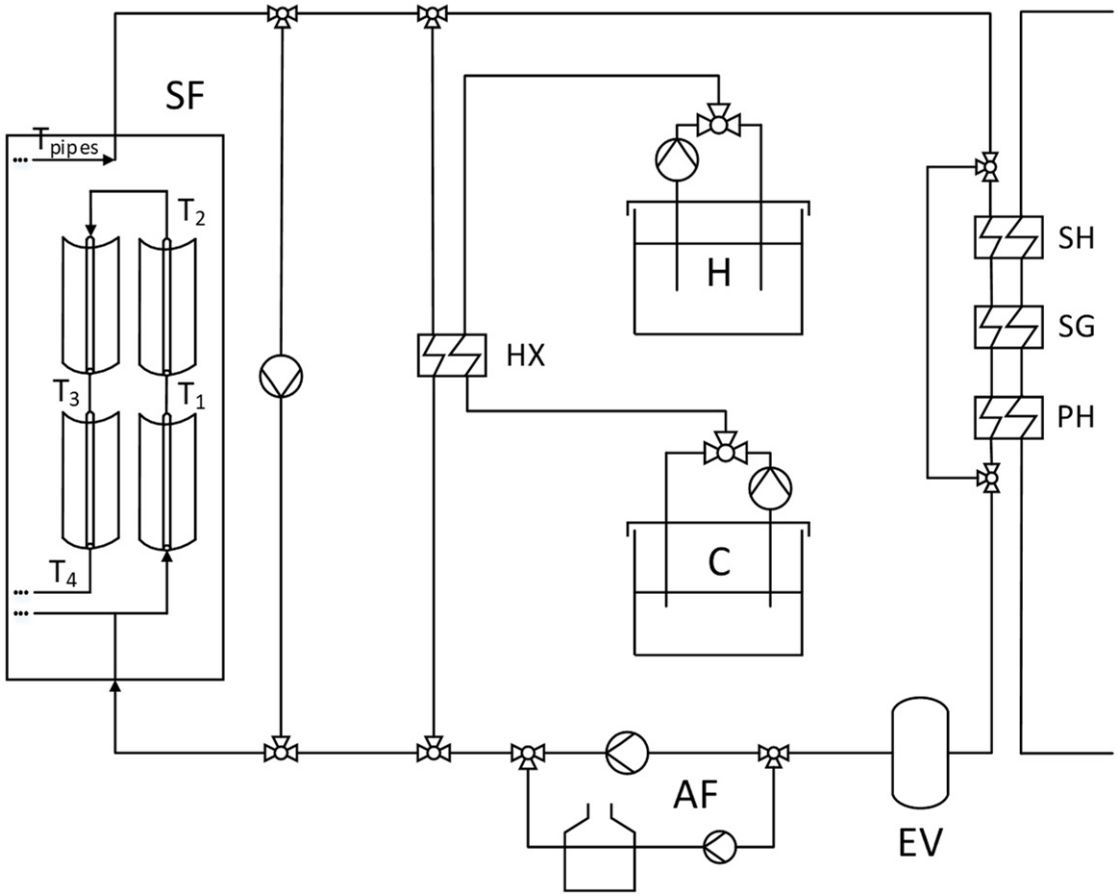

Figure 1. Scheme of the solar field (adapted from [32]). Each loop consists of 4 SCAs in series formed by 12 SCEs, each one with 36 HCEs. The field is composed of 156 loops in parallel. SF = solar field; HX = heat exchanger; H = hot tank; C = cold tank; AF = anti-freeze system; EV = expansion vessel.

For the sake of brevity, only the representative equations of the model are presented hereafter. The solar time, t_{solar}, is calculated with Equation (1):

$$t_{solar} = t_h + \frac{t_{min}}{60} + \frac{(\lambda - \lambda_{TZM})}{15} + \frac{EOT}{60} - DS \quad (1)$$

where λ is the longitude of the plant location in degrees, λ_{TZM} is the longitude of the time zone meridian, EOT is the equation of time in minutes, and DS is the daylight savings.

The useful thermal power absorbed by each loop of the solar field, $P_{absLoop}$, is determined through Equation (2):

$$P_{absLoop} = E_b \cdot A_c \cdot \cos(\theta) \cdot \eta_{opt,0} \cdot K_{iam}(\theta) \cdot f_{RowShadow} \cdot f_{endLoss} \cdot f_{clean} \cdot f_{dust} \cdot \eta_{track} \cdot f_1 \quad (2)$$

where E_b is the DNI, A_c is the mirror aperture area of each loop, θ is the incident angle, $\eta_{opt,0}$ is the peak optical efficiency of the collector, K_{iam} is the incidence angle modifier, $f_{RowShadow}$ is the row shadowing factor, $f_{endLoss}$ is the end loss factor, f_{clean} is the mirror cleanliness factor, f_{dust} is the dust factor, η_{track} is the tracking error, and f_1 is an extra factor accounting for any other thermal energy absorption reduction effect.

The HTF temperature in each collector, T_i, is calculated with the following equation:

$$T_i = \frac{T_{i,0} + \left(\frac{\dot{m}_{loop}}{\rho(T_{i,0}) V_{SCA}} T_{pipes,0} + \frac{P_{usefulLoop}/4}{\rho(T_{i,0}) V_{SCA} c_p(T_{i,0})} \right) \Delta t}{\left(1 + \frac{\dot{m}_{loop}}{\rho(T_{i,0}) V_{SCA}} \Delta t \right)} \quad (3)$$

where $T_{i,0}$ is the temperature at the beginning of the time interval, $\dot{m}_{loop}$ is the HTF mass flow rate in a collector loop, ρ is the HTF density, V_{SCA} is the HTF volume within the receiver tubes in an SCA, $T_{pipes,0}$ is the HTF temperature in the insulated pipes, $P_{usefulLoop}$ is the useful thermal power absorbed by the loop, c_p is the HTF specific heat at constant pressure, and Δt is the time interval.

The power cycle subsystem. It consists of a regenerating Rankine cycle (Figure 2) with reheat, which consists of a train of heat exchangers (preheater (PH), steam generator (SG), superheater (SH), and reheater (RH)); a high-pressure turbine (HP); a low-pressure turbine (LP); and five feedwater preheaters (FWH1–5), including a deaerator, a condensate pump (CP), and a high-pressure/main pump (MP). The multi-effect distillation unit replaces the power cycle condenser. The nominal thermal performance is calculated for the aforementioned configuration. Regarding the operation of this subsystem out of the nominal conditions, the power curve as a function of the thermal power input given by Llorente et al. [32] has been adopted considering the nominal point calculated with the distillation unit integrated into the power block (Figure 3).

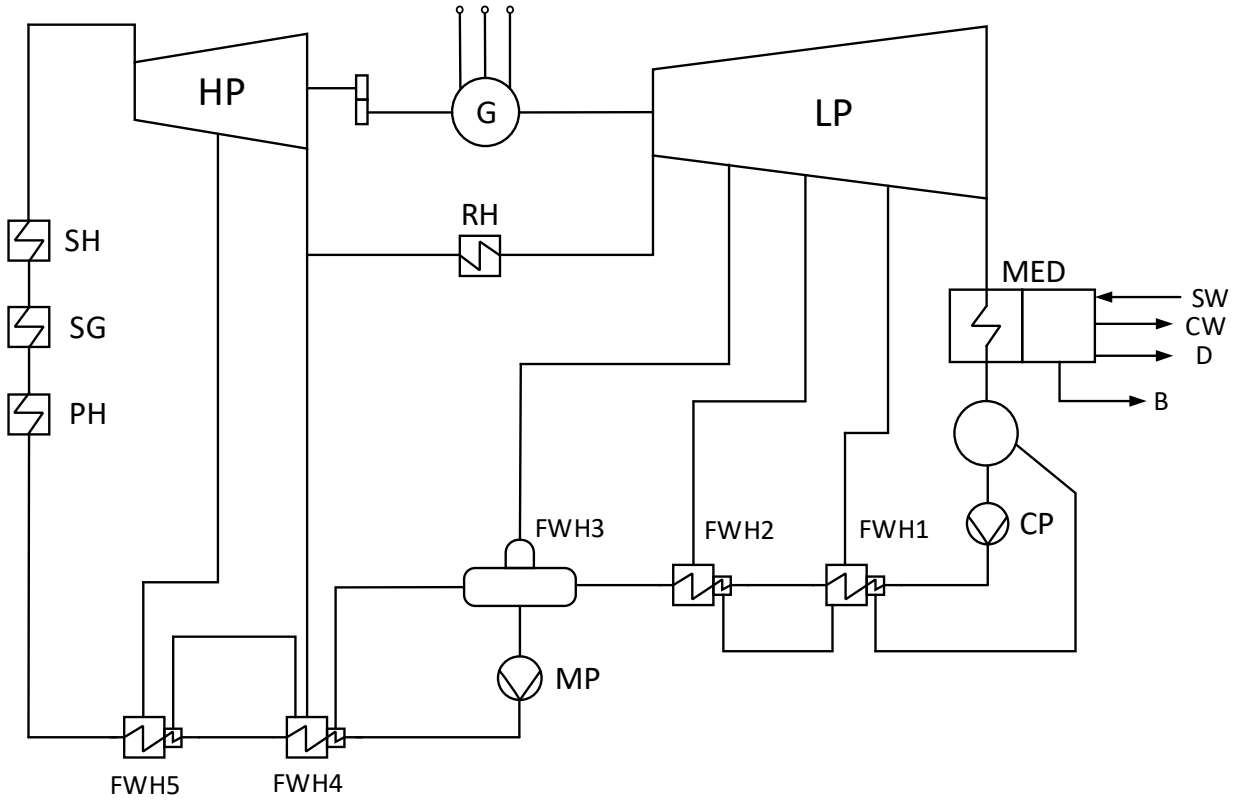

Figure 2. Power block scheme with the MED acting as the condenser of the cycle. PH = preheater; SG = steam generator; SH = superheater; HP = high-pressure turbine; G = electric generator; RH = reheater; LP = low-pressure turbine; CP = condensate pump; MP = main pump; FWH = feed water heater; SW = seawater; CW = cooling water; D = distillate; B = brine.

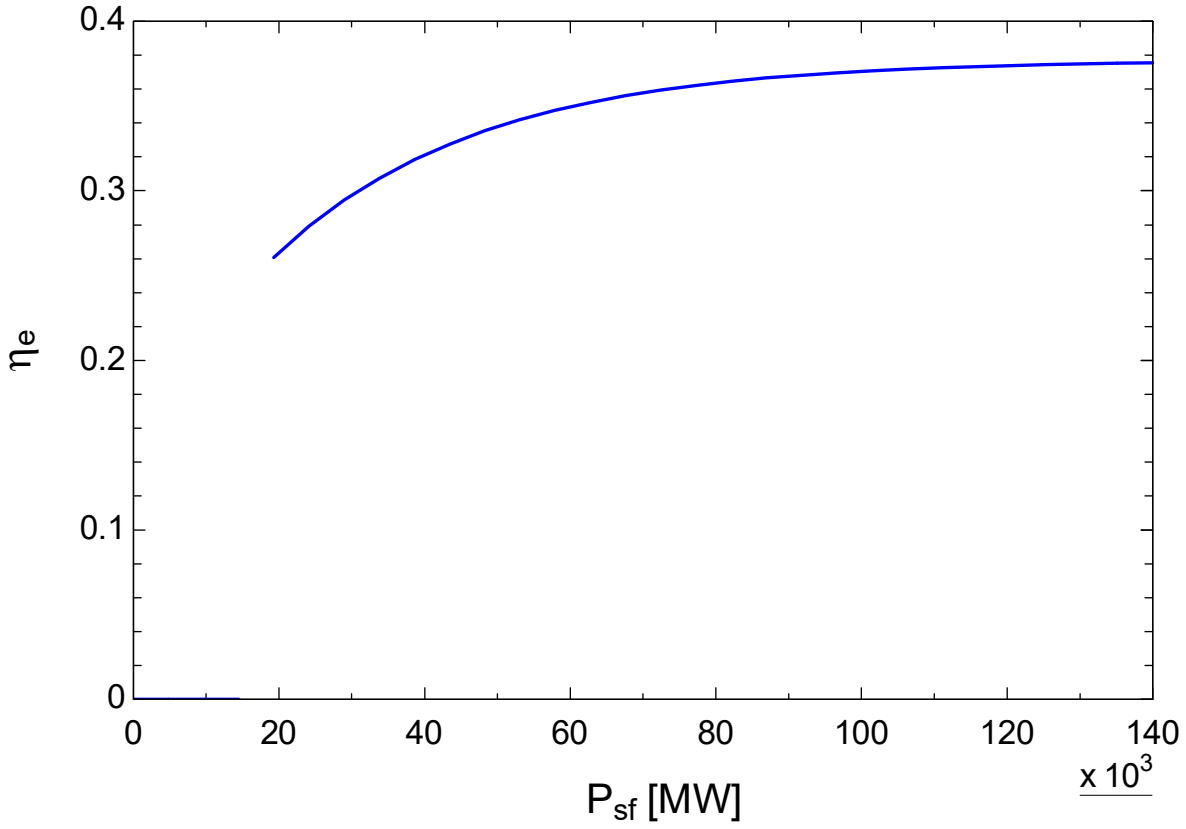

Figure 3. Electric efficiency of the power block as a function of the useful thermal power from the solar field (P_{sf}).

The model of the power block was developed on the basis of mass and energy balances applied to each component of the plant. The efficiency of the turbines, η_T, is determined with

$$\eta_T = \frac{h_{in} - h_{out}}{h_{in} - h_{out,s}} \tag{4}$$

where h_{in} is the specific enthalpy of the steam at the inlet of the turbine, h_{out} is the specific enthalpy of the steam at the outlet of the turbine, and $h_{out,s}$ is the isentropic specific enthalpy of the steam (with respect to the inlet). Steam pressures extractions are selected so that the same enthalpy difference is obtained in each preheater. The efficiency of the power block (defined as the fraction of thermal power converted to electricity) (Figure 3) is calculated through Equation (5):

$$\eta_e = \begin{cases} 0, & P_{sf} \leq 19\ MW \\ \alpha \cdot \left(a_1 + a_2 \exp\left(\dfrac{-P_{sf}}{a_3} \right) \right), & P_{sf} > 19\ MW \end{cases} \tag{5}$$

where α is equal to 0.95 (accounts for the reduction of the efficiency due to the condensation at 70 °C); a_1, a_2, and a_3 are constants equal to 0.397, −0.243, and 28,230, respectively; and P_{sf} is the solar field thermal power ($= P_{usefulLoop} \cdot N_{loops}$). Note that 19 MW is the minimum thermal power considered to start the turbine operation. The gross electric power delivered by the power block, $P_{e,gross}$, is determined with Equation (6):

$$P_{e,gross} = \eta_{HX,PB} P_{sf} \eta_e \tag{6}$$

where $\eta_{HX,PB}$ is the efficiency of the power block heat exchanger.

The seawater desalination subsystem. The performance of the MED unit, given by the gain output ratio (GOR, defined as the mass flow rate of distillate produced per kg/s of heating steam consumed), is assumed to be constant with the external steam variation in the first effect. Although there is a little drop in the GOR, the influence of the time step in the yearly production is not affected by this assumption. It has been considered a constant GOR of 8, related to a 10-effect MED [34]. The distillate produced by the MED, q_D, is calculated as follows:

$$q_D = GOR \cdot q_{cond} \quad (7)$$

where q_{cond} is the mass flow rate of exhaust vapor from the last section of the low-pressure turbine. Conceptually, the time step may have the lowest influence on production results in clear days since the solar irradiance exhibits the lowest variability. Besides that, on completely cloudy days, the irradiance has wide periods with constant and low values. On the contrary, days with short cloudy periods show the highest variability. Therefore, the minimum influence of the time step should be found in clear days.

The model of the integrated system has been implemented in Engineering Equation Solver (EES) [35]. It divides a day into four different periods: the first period corresponds to the night before the sunrise, the second describes the warm-up of HTF in the solar field and start-up of the turbine, the third period of full operation, and finally the night period after the sunset. Only when the temperature in the insulated pipes (T_{pipes}) reaches 310 °C (390 °C − ΔT_{margin}, with ΔT_{margin} = 80 °C) does the start-up of the turbine and the electricity generation ($P_{e,gross}$) begin. The model requires setting up the initial conditions to be solved, which is related to the HTF temperatures in each collector and insulated pipe.

The main assumptions considered for the models are:

- Any pressure change of the HTF within the solar field pipes is neglected.
- All the solar field loops are considered to be identical.
- A linear and discrete approximation of the differential equations obtained from the energy balance in the SF pipes is assumed.
- The variation of the density and specific heat of the HTF is neglected in a short time interval.
- A power block efficiency curve is assumed for the operation of the system.
- A constant GOR of 8 is assumed for a MED of 10 effects, neglecting any variation of the efficiency with respect to the mass flow rate of heating steam introduced.

A comparative assessment of the power and water production of the CSP+D plant as a function of the time step is carried out. Firstly, the combined production for different time steps is analyzed, and then two cases (5 min and 1 h time steps) are studied for one clear day. After that, the main performance parameters are comparatively evaluated for three consecutive days in summer. Finally, the yearly production is estimated using 5 min and 1 h time step simulations.

3. Results and Discussion

A representative set of results are presented in this section. Table 1 details the results obtained of the electric gross energy (E_{gross}) and freshwater production (q_d) for the time steps (Δt) considered (5, 10, 15, 30 min and 1 h) during three days in summer, 21–23 June. The relative errors committed for E_{gross} (ε_E) and q_d (ε_{qd}), taking as reference value the 5 min simulation results, are also shown. This information quantifies the sub-estimation of both energy and water production when the time step of the simulation is greater than 5 min. The reference case corresponds to the 5 min simulation, where the results for the gross electric energy and freshwater produced are 2.19 GWh and 48.2 hm^3, respectively. If the simulation time step is increased to 10, 15, 30, and 60 min the amount of energy and water collected decreases gradually, reaching a descent of 30.3% in the latter case. This shows that simulations of the dual-purpose plant performed with a time step of 1 h are not suitable with the CSP model used. Furthermore, lowering the time step results in better estimates at the expense of increasing the calculation time (t_{calc}) exponentially.

Table 1. Simulation of the electric gross energy (E_{gross}) and freshwater production (q_d) as a function of the time step (Δt) during three days in summer: 21–23 June 21. ε_E and ε_{qd} are the relative errors of E_{gross} and q_d, respectively.

Period	Δt	t_{calc}	E_{gross}	ε_E	q_d	ε_{qd}
	min	min	GWh	%	hm^3	%
21–23 June	5	43.59	2.19	-	48.2	-
	10	13.17	2.13	2.4	47.0	2.4
	15	4.75	2.08	4.8	45.9	4.8
	30	1.02	1.93	11.9	42.5	11.8
	60	0.12	1.52	30.3	33.9	29.7

3.1. Comparison for One Clear Day with 5 min and 1 h Time Steps

A comparison of the direct normal irradiance (DNI), E_b, and gross electric power, $P_{e,gross}$, simulated with 5 min and 1 h time steps for a clear day in summer (22 June) is shown in Figure 4. The simulation was extended to 28 h in order to take into account the possible operation at night due to the TES system. Note how the 5 min DNI curve is more detailed and has more peaks than the 1 h curve, which will eventually affect the heat transfer fluid temperatures in the solar field and therefore the gross electric energy produced. The 5 min simulation takes more points in the same time interval, leading to a more accurate description of the process. As the algorithm splits the day into four periods, taking a small enough step time results in a sooner response of the HTF temperature and therefore a faster startup of the electric energy production. In addition, the gross electric power curve simulated with the 1 h time step rises later and descends earlier than in the 5 min time step case because the TES system stores less energy.

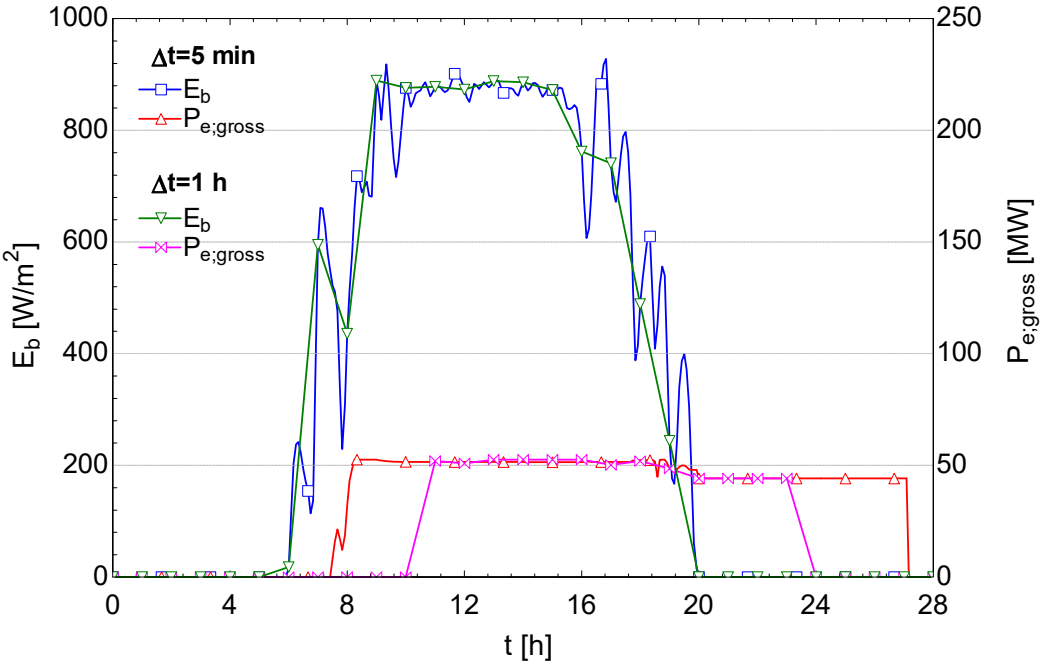

Figure 4. Comparison of the direct normal irradiance (E_b) and gross electric power production ($P_{e,gross}$) obtained with 5 min and 1 h time step simulations for 22 June.

As can be seen in Figure 5, the HTF temperature in the insulated tubes (T_{pipes}) is achieved 310 °C earlier in the 5 min time step simulation than in the 1 h time step simulation and thus it is possible to produce energy earlier in the power block. Moreover, the TES system is also charged before and up to its maximum ($E_{stored,total}$ = 1010 MWh) thanks to the excess of thermal energy in the solar field ($P_{PB,excess}$), which in turn leads to a long

energy production after the sunset (≈20 h) than in the case of the simulation with 1 h step time. Note that the maximum power sent from the TES system to the Power Block ($P_{TEStoPB}$) was limited to 119 MW, and from the solar field to 140 MW. Note also how the useful thermal power obtained by the SF ($P_{SF,useful}$) takes place approximately from 8 h to 20 h, matching the DNI availability.

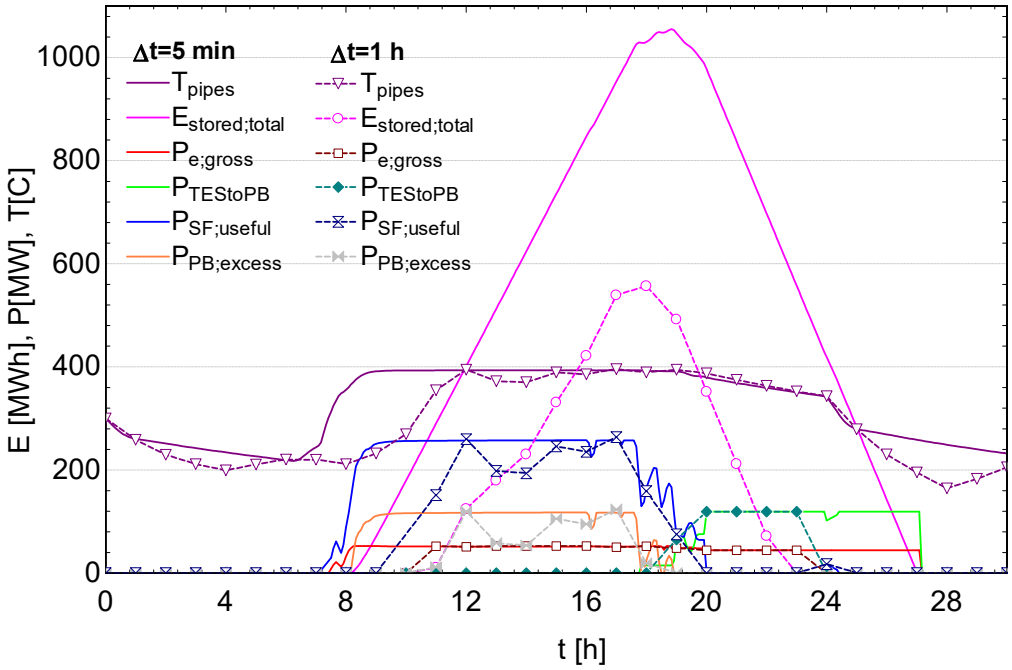

Figure 5. Comparison of the HTF temperature (T_{pipes}), energy stored in the TES (E_{stored}), gross electric power ($P_{e,gross}$), thermal power sent from the TES ($P_{TEStoPB}$), useful thermal power from the SF ($P_{SF,useful}$), and excess of thermal power ($P_{PB,excess}$), with 5 min and 1 h time steps simulations for 22 June.

3.2. Comparison for Three Days with 5 min and 1 h Time Steps

Figures 6 and 7 compare the simulation results of three consecutive days in summer, 21–23 June, using a 5 min TMY for the proposed location. The first day has a very irregular DNI profile that could correspond to a cloudy day with intermittent periods of clear. The other two days are typical days of summer with good and nearly regular DNI levels. As a result of taking a small time step for the iterative process that calculates the HTF temperature in the solar field, the temperature profiles are almost fully developed, thus producing a higher amount of energy in the power block. Freshwater production in the desalination unit should have a similar trend. For the 1 h time step simulation, temperature profiles are very irregular, and then the rest of the variables are influenced by this effect, resulting in an underestimation of the electric energy produced.

Figure 8 shows the motive steam and accumulated freshwater production for the three consecutive days selected of summer (21–23 June), with time steps of 5 min and 1 h. The deviation found in the 1 h simulation is about 30% of the 5 min simulation. It is clear that for a suitable prediction of the amount of water produced, a low time step needs to be chosen. The use of a non-dynamic model for the distillation unit leads to a small deviation in the MED production. Since the objective of this work is to carry out a comparison, the freshwater production decrease due to the off-design operation of the plant will have no impact on the results.

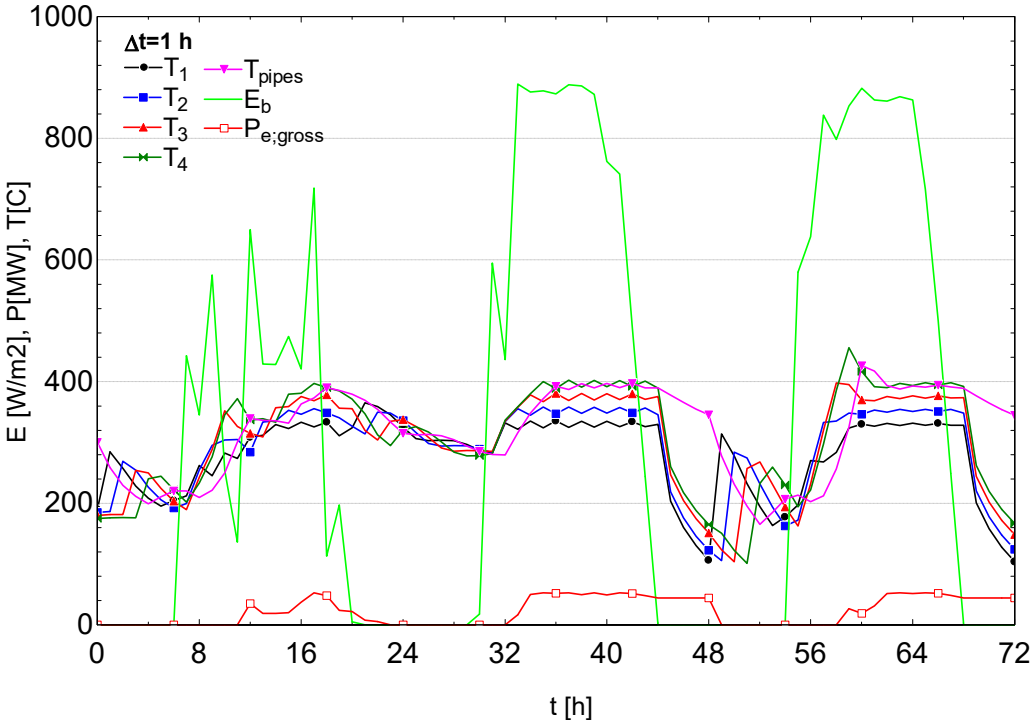

Figure 6. Simulation of direct normal irradiance (E_b), HTF temperatures in a generic loop (T_i), and gross electric power ($P_{e,gross}$) for three days in summer, 21–23 June with a time step of 1 h.

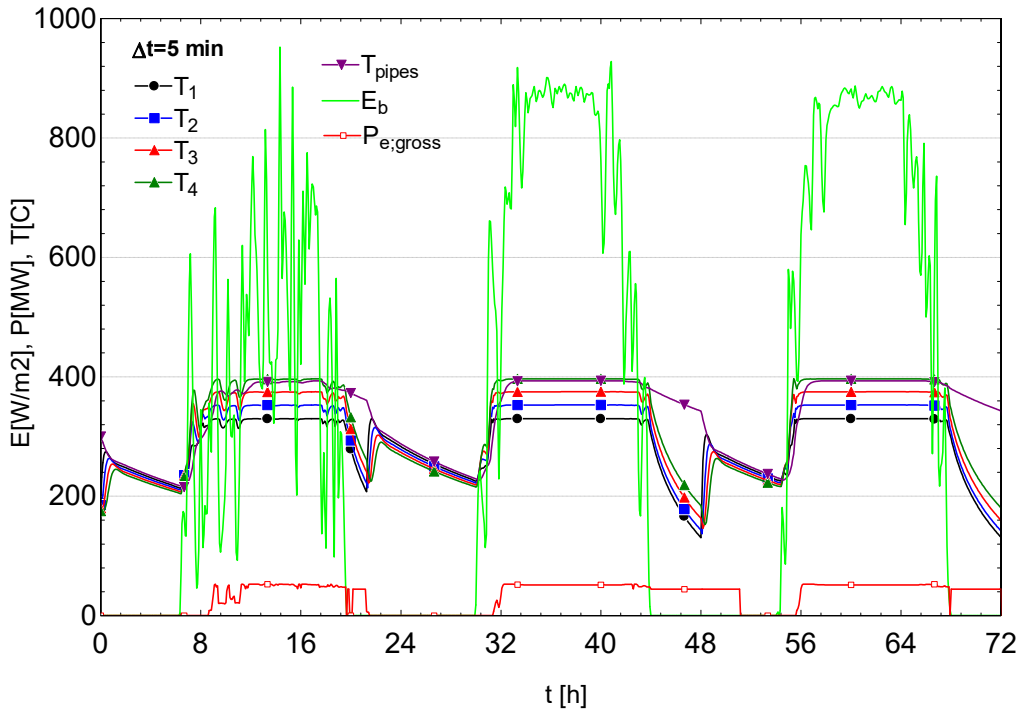

Figure 7. Simulation of direct normal irradiance (E_b), SCA HTF temperatures (T_i), and gross electric power ($P_{e,gross}$) for three days in summer, 21–23 June, with a time step of 5 min.

The nominal steam mass flow rate at full operation is about 37.17 kg/s in solar-only mode, with a freshwater flow rate of 1070 m^3/h. After the sunset, the TES system starts to operate with a limitation in the maximum power sent to the power block (119 MW), thus resulting in lower efficiency and less motive steam available for the MED production. This

is the reason for the step observed in Figure 9. The new nominal values in this period are 32.23 kg/s and 928.26 m^3/h of steam and water, respectively.

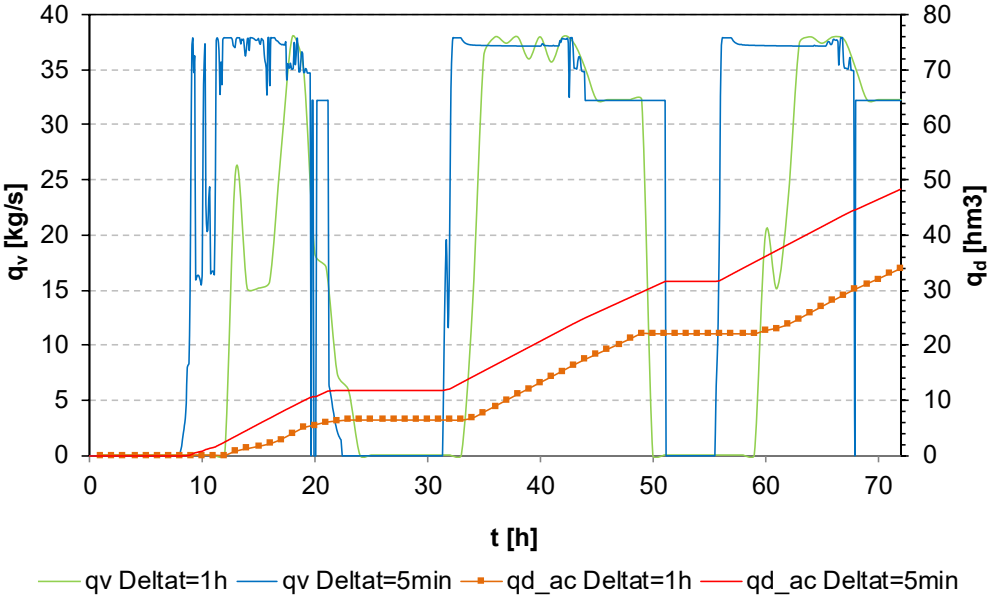

Figure 8. Simulation results for the freshwater mass flow rate (q_v) and freshwater volume (q_d) for three days in summer, 21–23 June, with 5 min and 1 h time steps.

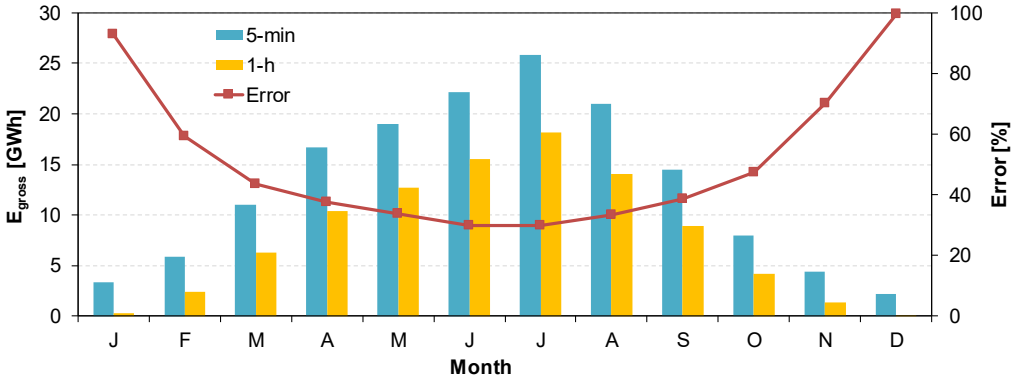

Figure 9. Yearly production of gross electric energy obtained with 5 min and 1 h simulation time steps.

3.3. Annual Power and Freshwater Comparison

Table 2 presents the gross electric energy (E_{gross}) and freshwater production (q_d) obtained when simulating one year using two different time steps, 5 min and 1 h. The relative errors in the electric power (ε_E) and freshwater production (ε_{qd}) estimations with the 1 h simulation are also shown, wherein the exact value was considered that of the 5 min simulation. Figures 9 and 10 show the evolution of the gross electric energy and freshwater production on a full-year basis, month by month.

The estimated electric energy production during a year using a simulation with a step time of 1 h has an error of about 100% during the winter period, while this error reaches a minimum of 30% in summer (Figure 9). The same trend is observed in freshwater production (Figure 10). As expected, the high variability of the DNI in winter days has a major influence on the estimated production when a larger time step was used in the simulation. However, clear days of summer produced the lowest underestimation because of the regular DNI profiles during these days. It is recommended to select a 5 min or 10 min time step instead of 1 h to obtain a good level of accuracy in CSP models as the one used in this work. The model implemented is suitable for these short simulation time steps.

Table 2. Monthly electric gross energy (E_{gross}) and freshwater production (q_d) as a function of the time step during a year of operation. ε_E and ε_{qd} are the relative errors of E_{gross} and q_d, respectively.

Month	5 min		1 h			
	E_{gross}	q_d	E_{gross}	q_d	ε_E	ε_{qd}
	GWh	$\times 10^3$ m^3	GWh	$\times 10^3$ m^3	%	%
January	3.35	80.5	0.24	6.4	92.8	92.1
February	5.84	131.8	2.37	56.2	59.3	57.3
March	11.01	249.0	6.23	140.6	43.4	43.5
April	16.67	373.0	10.41	219.9	37.6	41.1
May	19.04	424.9	12.64	280.8	33.6	33.9
June	22.16	495.5	15.52	343.4	30.0	30.7
July	25.85	578.0	18.12	398.9	29.9	31.0
August	21.00	465.4	14.01	310.3	33.3	33.3
September	14.47	321.0	8.87	197.8	38.7	38.4
October	7.97	179.1	4.20	98.6	47.3	44.9
November	4.40	102.5	1.32	34.0	70.1	66.8
December	2.19	52.9	≈0	0.2	99.7	99.7
Year	153.95	3453.7	93.94	2087.1	39.0	39.6

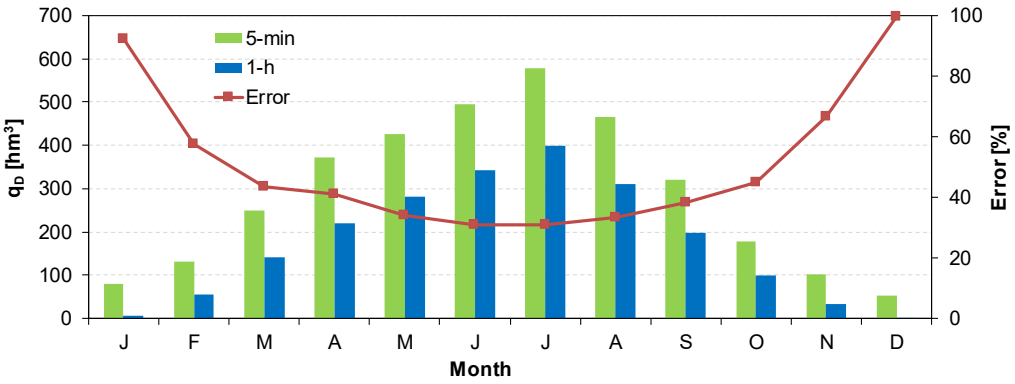

Figure 10. Yearly production of freshwater obtained with 5 min and 1 h simulation time steps.

4. Conclusions

This paper quantifies the influence of the time step of solar irradiance data on the power and the freshwater produced by a PT-CSP plant performing yearly simulations using a dynamic model. For the case study considered, 154 GWh and 3.45 hm^3 of power and water production were obtained using 5 min time steps, respectively, while 94 GWh and 2.1 hm^3 were obtained with 1 h time steps, respectively. Results reported deviations around 30% in clear days of June when the time steps selected were either 5 min or 1 h. Such a high deviation is consistent with the annual deviation found in the literature for other specific applications [11]. Given the high influence identified for this time step, future analysis is required on finding appropriate decision criteria.

The yearly production of electric energy and freshwater is not correctly estimated using a 1 h simulation time step using the detailed dynamic model presented in this work, which is sub-estimated by approximately 30% during summer days and 100% during winter days, taking a 5 min simulation as the reference case. This CSP model is prepared to take into account small disturbances in the DNI; therefore, using a 1 h simulation time step leads to losing relevant information in the plant operation strategy. A possible compromise solution between the calculation time and level of accuracy in this particular analysis could be to normalize the input DNI so that it remains the same for every time step, although the operating strategy of the plant is lost.

Moreover, a related aspect that requires further analysis is the imprecision of calculations based on average values of a typical meteorological year, especially in months with

numerous cloudy intervals. Further investigation on the use of TMY for estimating the yearly power and water production in CSP+D plants is recommended.

Author Contributions: Conceptualization, B.O.-D. and P.P.; methodology, B.O.-D. and P.P.; software, B.O.-D.; validation, B.O.-D. and P.P.; formal analysis, B.O.-D. and P.P.; investigation, B.O.-D. and P.P.; data curation, B.O.-D.; writing—original draft preparation, B.O.-D.; writing—review and editing, B.O.-D., P.P. and D.-C.A.-P.; visualization, B.O.-D.; supervision, D.-C.A.-P.; funding acquisition, D.-C.A.-P. All authors have read and agreed to the published version of the manuscript.

Funding: This research was funded by the European Regional Development Fund, Interreg Atlantic Area, and the EERES4WATER Project (Second Call, Priority 2, EAPA_1058/2018).

Institutional Review Board Statement: Not applicable.

Informed Consent Statement: Not applicable.

Data Availability Statement: Not applicable.

Acknowledgments: Diego-César Alarcón-Padilla wishes to thank the European Regional Development Fund, Interreg Atlantic Area, for its financial assistance within the framework of the EERES4WATER Project (Second Call, Priority 2, EAPA_1058/2018).

Conflicts of Interest: The authors declare no conflict of interest. The funders had no role in the design of the study; in the collection, analyses, or interpretation of data; in the writing of the manuscript; or in the decision to publish the results.

Nomenclature

E_b	Direct normal irradiance, W/m^2
E_{gross}	Gross electric energy, MWh
$E_{stored,total}$	Thermal energy stored in the TES system, MWh
ε_{E}	Relative error in the electric energy produced
$\varepsilon_{\mathrm{qd}}$	Relative error in the freshwater produced
$P_{e,gross}$	Gross electric power, MW
P_{field}	Useful thermal power obtained from the solar field, MW
$P_{PB,excess}$	Excess of thermal power in the solar field, MW
$P_{TEStoPB}$	Thermal power sent from the TES system to the power block, MW
q_v	Mass flow rate of steam in the first cell of the MED unit, kg/s
q_d	Freshwater volume produced in the MED unit, m^3
T_i	Heat transfer fluid temperature in SCA i, °C
ΔT_{margin}	Temperature margin from the design loop outlet temperature (390 °C)
Δt	Simulation time step, s
t_{calc}	Calculation time, s
Abbreviations	
AF	Anti-freeze
C	Cold tank
CSP+D	Concentrating solar power and desalination
CP	Condensate pump
DNI	Direct normal irradiance
EV	Expansion vessel
FWH	Feedwater heater
G	Electric generator
GOR	Gain output ratio
H	Hot tank
HCE	Heat collection element
HP	High-pressure turbine
HTF	Heat transfer fluid
HX	Heat exchanger

LP	Low-pressure turbine
MED	Multi-effect distillation
MP	Main pump
LT-MED	Low-temperature multi-effect distillation
PH	Preheater
PT-CSP	Parabolic trough concentrating solar power
RO	Reverse osmosis
RH	Reheater
SAM	Solar advisor model
SCA	Solar collector assembly
SCE	Solar collector element
SEGS	Solar energy generating system
SF	Solar field
SG	Steam generator
SH	Superheater
TES	Thermal energy storage
TMY	Typical meteorological year

References

1. IEA World Electricity Final Consumption by Sector, 1974–2019—Charts—Data & Statistics—IEA. Available online: https://www.iea.org/data-and-statistics/charts/world-electricity-final-consumption-by-sector-1974-2019 (accessed on 24 January 2022).
2. Palenzuela, P.; Zaragoza, G.; Alarcón-Padilla, D.C.; Guillén, E.; Ibarra, M.; Blanco, J. Assessment of different configurations for combined parabolic-trough (PT) solar power and desalination plants in arid regions. *Energy* **2011**, *36*, 4950–4958. [CrossRef]
3. Palenzuela, P.; Zaragoza, G.; Alarcón, D.; Blanco, J. Simulation and evaluation of the coupling of desalination units to parabolic-trough solar power plants in the Mediterranean region. *Desalination* **2011**, *281*, 379–387. [CrossRef]
4. Sharaf, M.A.; Nafey, A.S.; García-Rodríguez, L. Exergy and thermo-economic analyses of a combined solar organic cycle with multi effect distillation (MED) desalination process. *Desalination* **2011**, *272*, 135–147. [CrossRef]
5. Uche, J.; Valero, A.; Serra, L.; Torres, C. Bblocks software for thermoeconomic analysis of dual-purpose power and desalination plants. *Int. J. Thermodyn.* **2012**, *15*, 215–220.
6. Darwish, M.A.; Darwish, A. Solar cogeneration power-desalting plant with assisted fuel. *Desalin. Water Treat.* **2014**, *52*, 9–26. [CrossRef]
7. Ortega-Delgado, B.; García-Rodríguez, L.; Alarcón-Padilla, D.C. Thermoeconomic comparison of integrating seawater desalination processes in a concentrating solar power plant of 5 MWe. *Desalination* **2016**, *392*, 102–117. [CrossRef]
8. Ortega-Delgado, B.; Palenzuela, P.; Alarcón-Padilla, D.C.; García-Rodríguez, L. Quasi-steady state simulations of thermal vapor compression multi-effect distillation plants coupled to parabolic trough solar thermal power plants. *Desalin. Water Treat.* **2016**, *57*, 23085–23096. [CrossRef]
9. Leiva-Illanes, R.; Escobar, R.; Cardemil, J.M.; Alarcón-Padilla, D.C. Thermoeconomic assessment of a solar polygeneration plant for electricity, water, cooling and heating in high direct normal irradiation conditions. *Energy Convers. Manag.* **2017**, *151*, 538–552. [CrossRef]
10. Calise, F.; Dentice d'Accadia, M.; Vanoli, R.; Vicidomini, M. Transient analysis of solar polygeneration systems including seawater desalination: A comparison between linear Fresnel and evacuated solar collectors. *Energy* **2019**, *172*, 647–660. [CrossRef]
11. Walkenhorst, O.; Luther, J.; Reinhart, C.; Timmer, J. Dynamic annual daylight simulations based on one-hour and one-minute means of irradiance data. *Sol. Energy* **2002**, *72*, 385–395. [CrossRef]
12. Bonilla, J.; Yebra, L.J.; Dormido, S.; Zarza, E. Parabolic-trough solar thermal power plant simulation scheme, multi-objective genetic algorithm calibration and validation. *Sol. Energy* **2012**, *86*, 531–540. [CrossRef]
13. Lippke, F. *Simulation of the Part-Load Behavior of a 30 MWe SEGS Plant*; Sandia National Lab. (SNL-NM): Albuquerque, NM, USA, 1995.
14. Wagner, M.J.; Zhu, G. *Generic CSP Performance Model for NREL's System Advisor Model*; National Renewable Energy Lab. (NREL): Golden, CO, USA, 2011.
15. Wagner, P.H. Thermodynamic Simulation of Solar Thermal Power Stations with Liquid Salt as Heat Transfer Fluid. Ph.D. Thesis, Technische Universität München, München, Germany, 2012.
16. Casimiro, S.; Cardoso, J.; Ioakimidis, C.; Farinha Mendes, J.; Mineo, C.; Cipollina, A. MED parallel system powered by concentrating solar power (CSP). Model and case study: Trapani, Sicily. *Desalin. Water Treat.* **2015**, *55*, 3253–3266. [CrossRef]
17. Moser, M.; Trieb, F.; Fichter, T.; Kern, J.; Hess, D. A flexible techno-economic model for the assessment of desalination plants driven by renewable energies. *Desalin. Water Treat.* **2015**, *55*, 3091–3105. [CrossRef]
18. Alikulov, K.; Xuan, T.D.; Higashi, O.; Nakagoshi, N.; Aminov, Z. Analysis of environmental effect of hybrid solar-assisted desalination cycle in Sirdarya Thermal Power Plant, Uzbekistan. *Appl. Therm. Eng.* **2017**, *111*, 894–902. [CrossRef]

19. Mata-Torres, C.; Escobar, R.A.; Cardemil, J.M.; Simsek, Y.; Matute, J.A. Solar polygeneration for electricity production and desalination: Case studies in Venezuela and northern Chile. *Renew. Energy* **2017**, *101*, 387–398. [CrossRef]
20. Hoffmann, J.E.; Dall, E.P. Integrating desalination with concentrating solar thermal power: A Namibian case study. *Renew. Energy* **2018**, *115*, 423–432. [CrossRef]
21. Ortega-Delgado, B.; Palenzuela, P.; Alarcón-Padilla, D.C.; García-Rodríguez, L. Yearly simulations of the electricity and fresh water production in PT-CSP+MED-TVC plants: Case study in Almería (Spain). *AIP Conf. Proc.* **2018**, *2033*, 160004.
22. Askari, I.B.; Ameri, M. Solar Rankine Cycle (SRC) powered by Linear Fresnel solar field and integrated with Multi Effect Desalination (MED) system. *Renew. Energy* **2018**, *117*, 52–70. [CrossRef]
23. Palenzuela, P.; Ortega-Delgado, B.; Alarcón-Padilla, D.-C. Comparative assessment of the annual electricity and water production by concentrating solar power and desalination plants: A case study. *Appl. Therm. Eng.* **2020**, *177*, 115485. [CrossRef]
24. Al-Addous, M.; Jaradat, M.; Bdour, M.; Dalala, Z.; Wellmann, J. Combined concentrated solar power plant with low-temperature multi-effect distillation. *Energy Explor. Exploit.* **2020**, *38*, 1831–1853. [CrossRef]
25. Desai, N.B.; Pranov, H.; Haglind, F. Techno-economic analysis of a foil-based solar collector driven electricity and fresh water generation system. *Renew. Energy* **2021**, *165*, 642–656. [CrossRef]
26. Suraparaju, S.K.; Sampathkumar, A.; Natarajan, S.K. Experimental and economic analysis of energy storage-based single-slope solar still with hollow-finned absorber basin. *Heat Transf.* **2021**, *50*, 5516–5537. [CrossRef]
27. Suraparaju, S.K.; Dhanusuraman, R.; Natarajan, S.K. Performance evaluation of single slope solar still with novel pond fibres. *Process Saf. Environ. Prot.* **2021**, *154*, 142–154. [CrossRef]
28. Blanco-Marigorta, A.M.; Victoria Sanchez-Henríquez, M.; Peña-Quintana, J.A. Exergetic comparison of two different cooling technologies for the power cycle of a thermal power plant. *Energy* **2011**, *36*, 1966–1972. [CrossRef]
29. Montes, M.J.; Abánades, A.; Martínez-Val, J.M.; Valdés, M. Solar multiple optimization for a solar-only thermal power plant, using oil as heat transfer fluid in the parabolic trough collectors. *Sol. Energy* **2009**, *83*, 2165–2176. [CrossRef]
30. Xu, X.; Vignarooban, K.; Xu, B.; Hsu, K.; Kannan, A.M. Prospects and problems of concentrating solar power technologies for power generation in the desert regions. *Renew. Sustain. Energy Rev.* **2016**, *53*, 1106–1131. [CrossRef]
31. Ortega-Delgado, B.; Cornali, M.; Palenzuela, P.; Alarcón-Padilla, D.C. Operational analysis of the coupling between a multi-effect distillation unit with thermal vapor compression and a Rankine cycle power block using variable nozzle thermocompressors. *Appl. Energy* **2017**, *204*, 690–701. [CrossRef]
32. Llorente García, I.; Álvarez, J.L.; Blanco, D. Performance model for parabolic trough solar thermal power plants with thermal storage: Comparison to operating plant data. *Sol. Energy* **2011**, *85*, 2443–2460. [CrossRef]
33. Eck, M.; Barroso, H.; Blanco, M.; Burgaleta, J.I.; Dersch, J.; Feldhoff, J.-F.; Garcia-Barberena, J.; Gonzalez, L.; Hirsch, T.; Ho, C.; et al. guiSmo: Guidelines for CSP performance modeling—Present status of the SolarPACES Task-1 project. In Proceedings of the 17th SolarPACES Conference, Granada, Spain, 20–23 September 2011.
34. Ortega-Delgado, B.; García-Rodríguez, L.; Alarcón-Padilla, D.C. Opportunities of improvement of the MED seawater desalination process by pretreatments allowing high-temperature operation. *Desalin. Water Treat.* **2017**, *97*, 94–108. [CrossRef]
35. Klein, S. Engineering Equation Solver Software (EES) 2021. Version 11.212. Available online: https://fchartsoftware.com/ees/ (accessed on 31 January 2022).